RSC Advances

ROYAL SOCIETY OF CHEMISTRY

www.rsc.org/advances

Journal Name

RSCPublishing

COMMUNICATION

Cite this: DOI: 10.1039/x0xx00000x

Au nanoparticles supported on magnetically separable Fe_2O_3-graphene oxide hybrid nanosheets for the catalytic reduction of 4-nitrophenol

Hyunje Woo,[a] Ji Woong Kim,[b] Miran Kim,[a] Sungkyun Park[b] and Kang Hyun Park[*a]

Received 00th January 2012,
Accepted 00th January 2012

DOI: 10.1039/x0xx00000x

www.rsc.org/

A one-pot hydrothermal synthesis approach was developed to prepare $FeSO_4$•(H_2O)-graphene oxide (GO) nanosheets. Au nanoparticles were immobilized onto this support, giving Au/Fe_2O_3-GO nanocomposites. Fe_2O_3-GO supports showed high surface area and thermal stability. The Au/Fe_2O_3-GO and synthesized Au/Fe_3O_4 nanocomposites exhibited high catalytic activity and recyclability for the reduction of 4-nitrophenol.

4-Nitrophenol has been considered to be one of the most refractory pollutants in wastewaters generated by agricultural and industrial sources.[1] Until now, there have been many reports about applications of Au nanoparticles (NPs) on various supports as catalysts for the reduction of 4-nitrophenol, since the reduction product, 4-aminophenol, is an important intermediate for the manufacture of many analgesic and antipyretic drugs.[2,3] Among these studies, those using water as a solvent under mild conditions have attracted much attention from the environmental viewpoint.

In recent years, various studies have been conducted into hybrid nanostructures in order to fabricate and synthesize multicomponent structures that can combine the physical and chemical properties of the individual components.[4,5] This enhanced functionality makes these hybrid nanostructures useful in many research fields such as magnetics, plasmonics, and semiconductors.[6] Among various hybrid nanostructures, noble metal NPs with metal oxide supports and graphene oxide (GO) have been applied to organic reactions as catalysts.[7-9] For instance, Zhao and coworkers[8] developed multi-functional mesoporous composite microspheres with well-designed nanostructures for an integrated catalyst system. Mülhaupt *et al.*[9] reported Pd NPs on graphite oxide and their functionalized graphene derivatives with the aim of creating a hybrid catalytic system. These hybrid nanocatalysts have the advantages of higher catalytic activity and better recyclability than are offered by single metal nanoparticles, owing to electron transfer across the interface as well as their heterogeneous properties.[10,11] In a number of supports, iron oxide and GO are important since iron oxide can be separated by an external magnet and GO has high electrical conductivity. Even though iron oxide supports show high recyclability, they are unstable in air and easily aggregate.[12] Moreover, taking advantage of surface functional groups as well as the large surface area of GO nanosheets,[13] they cannot be easily recycled by an external magnet; therefore, it is essential to combine advantages of iron oxide and GO. Our ongoing interest in the iron oxide-GO support combining both advantages of iron oxide and GO motivated us to investigate iron oxide-GO supports by a facile approach. In this study, we synthesized $FeSO_4$•(H_2O)-GO nanosheets by a one-pot method and then Au NPs were immobilized onto this support. During the immobilization of the Au NPs in situ, $FeSO_4$•(H_2O) transformed into Fe_2O_3, resulting in superparamagnetic Au/Fe_2O_3-GO nanosheets. To the best of our knowledge, this is the first example of a versatile synthesis of Au/Fe_2O_3-GO nanosheets. Au/Fe_2O_3-GO nanosheets were then used as a catalyst for the reduction of 4-nitrophenol in water, and high catalytic activity and recyclability were achieved.

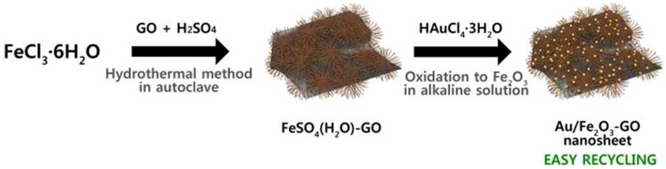

Scheme 1. Synthetic scheme of Au/Fe_2O_3-GO hybrid nanosheets.

The Au/Fe_2O_3-GO nanosheets were synthesized via two steps from $FeCl_3$•$6H_2O$ (Scheme 1). $FeSO_4$•(H_2O)-GO nanosheets were prepared by an in situ hydrothermal method.[14] A gold precursor was subsequently injected to yield Au/Fe_2O_3-GO nanosheets. GO nanosheets were used as the precursor to prepare $FeSO_4$•(H_2O)-GO nanocomposites, which were synthesized from natural graphite powders by a modified Hummer's method.[15] For comparison, Au/Fe_3O_4 microspheres were also synthesized.

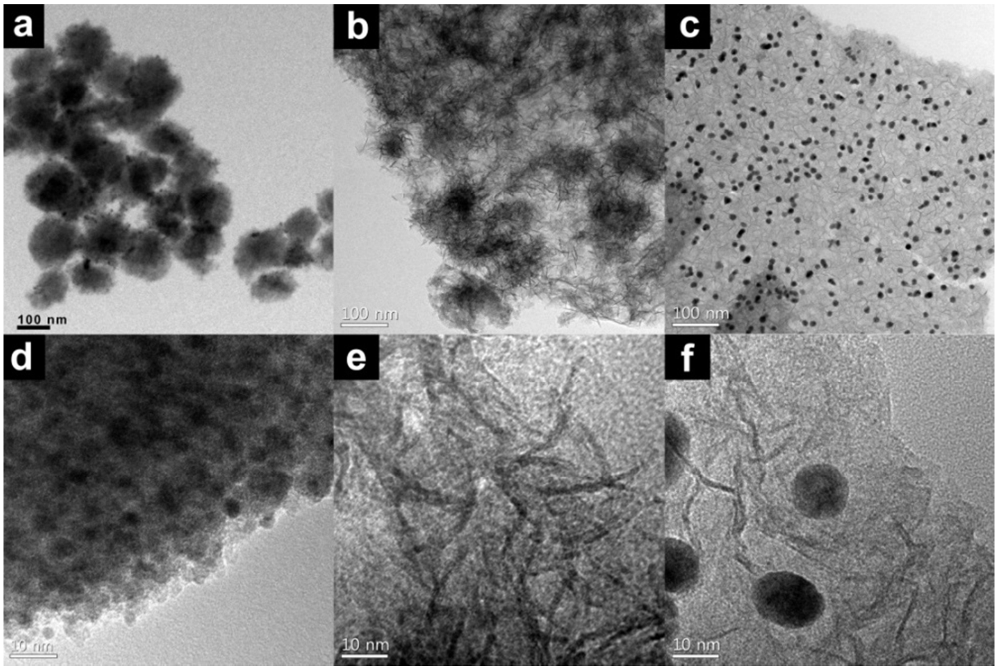

Fig. 1. TEM images of Au/Fe_3O_4 microspheres (a,d), $FeSO_4$•(H_2O)-GO (b,e) and Au/Fe_2O_3-GO nanosheets (c,f).

Transmission electron microscopy (TEM) images show the morphology of Au/Fe_3O_4 microspheres, $FeSO_4$•(H_2O)-GO and Au/Fe_2O_3-GO nanosheets (Fig. 1). Low-resolution TEM images of $FeSO_4$•(H_2O)-GO and Au/Fe_2O_3-GO nanosheets are shown in Fig. S1a,b (ESI†). Prior to the immobilization of the Au NPs onto the Fe_3O_4 microspheres, pretreatment procedures such as coating polymers or SiO_2 onto Fe_3O_4 were not required. In fact, the Au NPs were easily immobilized onto the surface of Fe_3O_4 in situ because of the interaction of the carboxyl groups of trisodium citrate with Au (Fig. 1a and 1d).[16] Size distribution graphs of the Au NPs are shown in Fig. S1c (ESI†), indicating the average size of the Au NPs was 8.0 nm. The x-ray diffraction (XRD) pattern of the Au/Fe_3O_4 microspheres matched the cubic spinel structure of Fe_3O_4 (JCPDS No. 19-0629) and face-centered cubic structure of Au (JCPDS No. 04-0784) (Fig. 2a).

The TEM images in Fig. 1b and 1e show $FeSO_4$•(H_2O)-GO nanocomposites. GO and $FeSO_4$•(H_2O)-GO were also imaged by non-tapping mode dynamic force microscope (DFM). Fig. S2 (ESI†) shows the DFM images of GO and $FeSO_4$•(H_2O)-GO, showing topology of nanocomposites. As shown in Fig. 2a, the XRD pattern shows anorthic $FeSO_4$•(H_2O) reflections (JCPDS No. 81-0019). Fourier-transform infrared (FT-IR) spectra were also measured to confirm the structure of GO and $FeSO_4$•(H_2O)-GO (Fig. 3). In the case of GO, the bands at ca. 1200 cm^{-1}, 1070 cm^{-1}, and 1720 cm^{-1} are attributed to the C–O epoxy stretching, C–O alkoxy stretching, and C=O carbonyl stretching vibrations, respectively; the absorption band at ca. 3450 cm^{-1} corresponds to O–H stretching.[17] Additionally, $FeSO_4$•(H_2O)-GO shows strong bands corresponding to $FeSO_4$•(H_2O). The asymmetric bending mode of SO_4^{2-} is presented as triplet at 606, 625, and 667 cm^{-1}. The asymmetric bending mode of OH^- is located at 555 and 823 cm^{-1}. The symmetrical stretching mode of SO_4^{2-} is registered at 1020 cm^{-1}. The asymmetrical stretching mode of SO_4^{2-} is split into two peaks, due to lower symmetry: 1080 and 1130 cm^{-1}. The symmetric bending modes of the hydroxyl group and crystal water are registered at 1500 and 1650 cm^{-1}, respectively. The broad band of OH^- in the range 3000–3500 cm^{-1} is associated with strong hydrogen bonds.[18] Elemental analysis of $FeSO_4$•(H_2O)-GO was confirmed by using X-ray photoelectron spectroscopy (XPS). The Fe^{2+} $2p_{3/2}$ peak of $FeSO_4$•(H_2O) is 710.9 eV; the binding energies of the doublet for S^{6+} $2p_{1/2}$ (168.1 eV) and S^{6+} $2p_{3/2}$ (168.6 eV) are shown in Fig. S3 (ESI†) and are consistent with the previously reported $FeSO_4$•(H_2O) data (Fig. S3a and S3c, ESI†).[19] In the case of GO, curve fitting of the C1s and O1s spectra was conducted using a Gaussian-Lorentzian function following Shirley background correction. The binding energy of the C–C is assigned at 284.3 eV and shifts of +1.6 and +3.3 eV are typically assigned to the C–OH and C=O functional groups, respectively (Fig. S3b, ESI†).[20]

In order to immobilize the Au NPs onto the $FeSO_4$•(H_2O)-GO support, a method of exchanging sodium cations with noble metallic ions was applied.[16] In alkaline aqueous solution, iron salts precipitate,[21] leading to the oxidation of $FeSO_4$•(H_2O) to Fe_2O_3 during immobilization of the Au NPs, resulting in Au/Fe_2O_3-GO nanosheets. TEM images show highly monodisperse Au NPs immobilized onto Fe_2O_3-GO nanosheets (Fig. 1c and 1f). Size distribution graphs of the Au NPs are displayed in Fig. S1d (ESI†), showing the average size of the Au NPs was 7.6 nm. Since it was difficult to assign the crystal structure of Fe_2O_3 due to the low intensity in the XRD pattern (Fig. 2a), we confirmed the Fe_2O_3 structure by using the XPS technique. In the case of high-spin iron, the Fe 2p peak is always split into two due to spin–orbit coupling (Fe $2p_{1/2}$, Fe $2p_{3/2}$). In the oxidized state (Fig. S3d, ESI†), an additional satellite peak appears in between the Fe $2p_{1/2}$ and Fe $2p_{3/2}$ components: for the case of Fe_2O_3, the satellite occurs 8 eV above the Fe $2p_{3/2}$ component.[22] The binding energy of the C–C is also assigned at 284.3 eV and shifts of +1.5 and +3.8 eV are typically assigned for the C–OH and C=O functional groups, respectively (Fig. S3e, ESI†).[20] When the Au/Fe_2O_3-GO nanosheets were synthesized, GO was further oxidized. The binding energies of the doublet for Au $4f_{7/2}$ (83.1 eV) and Au $4f_{5/2}$ (87.0 eV) shown in Fig. S3f (ESI†) are characteristic of Au^0.[23]

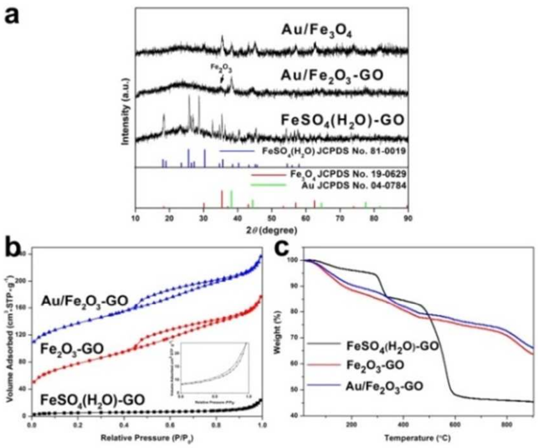

Fig. 2. (a) XRD graphs of FeSO$_4$•(H$_2$O)-GO, Au/Fe$_2$O$_3$-GO and Au/Fe$_3$O$_4$. (b,c) Nitrogen-adsorption/desorption isotherms and TGA data of FeSO$_4$•(H$_2$O)-GO, Fe$_2$O$_3$-GO and Au/Fe$_2$O$_3$-GO; for clarity, the isotherms of Fe$_2$O$_3$-GO and Au/Fe$_2$O$_3$-GO were shifted upwards by 50 and 110 cm^{3}g^{-1}, respectively.

As a control experiment, Fe$_2$O$_3$-GO nanosheets were also synthesized without addition of HAuCl$_4$•3H$_2$O. As shown in the N$_2$ adsorption/desorption isotherms (Fig. 2b), Fe$_2$O$_3$-GO and Au/Fe$_2$O$_3$-GO nanosheets showed typical IV isotherms, indicating the presence of mesopores (4.4 nm) and high surface area (292 m^{2}g^{-1}). The textural characteristics of the corresponding samples are summarized in Table S1 (ESI†). Surprisingly, the surface area of FeSO$_4$•(H$_2$O)-GO was less than 20 m^{2}g^{-1} (Table S1, ESI†). Thermogravimetric analysis (TGA) was then used to characterize the thermal stability of the three samples (Fig. 2c). TGA data also showed a different tendency of weight loss (%) between FeSO$_4$•(H$_2$O)-GO and Fe$_2$O$_3$-GO nanocomposites. It is considered that the physical and chemical properties of FeSO$_4$•(H$_2$O)-GO were drastically changed in alkaline solution during the Au NP immobilization. The elemental compositions of the respective Au/Fe$_3$O$_4$, FeSO$_4$•(H$_2$O), Fe$_2$O$_3$-GO, and Au/Fe$_2$O$_3$-GO nanocomposites were obtained using energy-dispersive X-ray spectroscopy (EDS) (Fig. S4, ESI†). The superconducting quantum interference device (SQUID) data showed the magnetic curves as a function of the applied field at 300 K (Fig. S5, ESI†). The saturation magnetization value of Au/Fe$_2$O$_3$-GO nanocomposites was 8.92 emu·g^{-1}, which was similar to that of the Fe$_2$O$_3$-GO (9.85 emu·g^{-1}). Moreover, both the remanence (Mr) and coercivity (Hc) of nanocomposites were close to zero, indicating superparamagnetism.

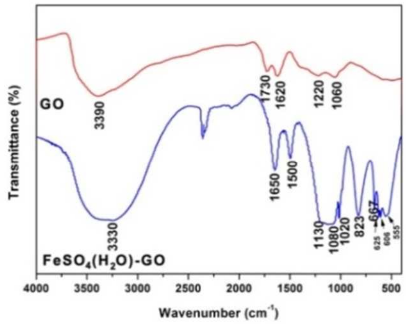

Fig. 3. The FT-IR spectra of GO and FeSO$_4$(H$_2$O)-GO nanosheets.

As shown in Fig. 4a and 4b, the UV/vis spectrum of the reaction mixture was monitored with time during the catalytic reduction of 4-nitrophenol. Specifically, the absorption of 4-nitrophenol at 400 nm decreased rapidly with a concomitant increase in the peak at 300 nm, that can be attributed to the formation of the reduction product, 4-aminophenol. The reduction was complete in 12 min and 6 min when Au/Fe$_2$O$_3$-GO (5.0 mol%) and Au/Fe$_3$O$_4$ (2.5 mol%) was used as the catalyst, respectively (100 equiv of NaBH$_4$ per equiv substrate at 298 K) (Fig. 4a and 4b). The real experimental absorption capacity of 4-nirophenol by Au/Fe$_2$O$_3$-GO is 1150 mg/g at the concentration of 104 mg/L, resulting in high adsorption capacity at room temperature. As shown in Fig. 4c, the Au/Fe$_3$O$_4$ catalyst showed a higher reaction constant k (0.284 min^{-1}) than the respective catalyst, Au/Fe$_2$O$_3$-GO (0.212 min^{-1}) nanocomposites. Slightly higher catalytic activity of the Au/Fe$_3$O$_4$ catalyst is attributed to its better dispersion stability in water. Because Fe$_3$O$_4$ has many citrate groups and OH$^-$ anions, the dispersion stability of Au/Fe$_3$O$_4$ in water is enhanced. As shown in Fig. 4d, the reaction rate constant k was also compared under different temperatures using 5.0 mol% of Au/Fe$_2$O$_3$-GO and 50 equiv of NaBH$_4$. As expected, the highest catalytic efficiency (0.252 min^{-1}) was obtained at 35 °C.

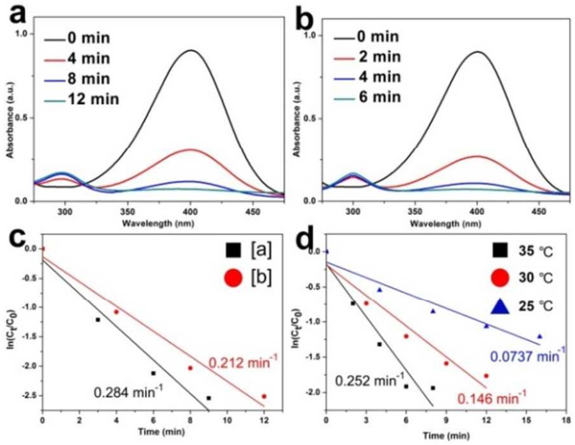

Fig. 4 Time-dependent UV/vis absorption spectra for the reduction of 4-nitrophenol over hybrid catalysts in aqueous media at 298 K. (a) Au/Fe$_2$O$_3$-GO (5.0 mol%). (b) Au/Fe$_3$O$_4$ (2.5 mol%). (c) Plot of ln(C$_t$/C$_0$) versus time with different catalysts. All catalysts are used at the same molar ratio of 5.0 mol% of catalyst and 100 equiv. of NaBH$_4$ for the reaction at R.T. [a] Au/Fe$_3$O$_4$ and [b] Au/Fe$_2$O$_3$-GO. (d) Plot of ln(C$_t$/C$_0$) versus time and the corresponding Arrhenius plot over Au/Fe$_2$O$_3$-GO catalysts under different temperatures at 5.0 mol% of catalyst and 50 equiv. of NaBH$_4$.

Both Au/Fe$_3$O$_4$ and Au/Fe$_2$O$_3$-GO catalysts exhibited superior catalytic activity relative to previously reported Au-Fe$_3$O$_4$ nanocomposites and Au/graphene nanosheets in terms of the reaction rate constant (k) value.[24,25] It is believed that the electronic structures of both the Au and the metal oxide components are modified by electron transfer across the interface of the Au–metal oxide hybrid NPs, giving rise to oxygen vacancies on the interfacial metal oxide that act as active sites for oxygen absorption and activation.[26,27] Thus, the hybrid NPs are catalytically more active than each individual component for the reduction of 4-nitrophenol.

Remarkably, after the reaction, the Au/Fe_2O_3-GO catalyst could be recovered from the reaction mixture by an external magnet and reused seven times with only slight loss of catalytic activity (Fig. 5a). Even though the Au/Fe_3O_4 catalyst showed higher catalytic activity than the Au/Fe_2O_3-GO catalyst, reusability of the Au/Fe_3O_4 catalyst was drastically decreased within four uses (Fig. 5b). As shown in Fig. S6 (ESI†), the structure of the Au NPs on the Fe_2O_3-GO nanosheets was slightly decomposed after the seven recycling reactions, demonstrating the recyclability of the catalyst.[28]

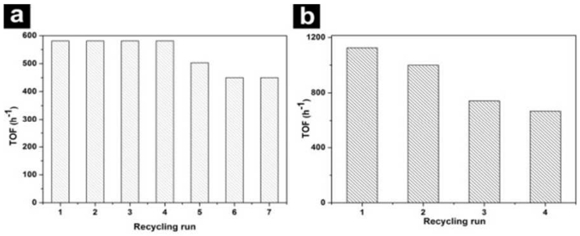

Fig. 5. (a) TOF during seven times recycling runs. Reaction condition: Au/Fe_2O_3-GO catalyst (Au base: 5.0 mol%), 200 equiv. of $NaBH_4$ and 35 °C. (b) TOF during four times recycling runs. Reaction condition: Au/Fe_3O_4 catalyst (Au base: 5.0 mol%), 200 equiv. of $NaBH_4$ and 35 °C.

In conclusion, $FeSO_4$•(H_2O)-GO nanosheets were synthesized by a one-pot method and Au NPs were immobilized onto this support, giving an Au/Fe_2O_3-GO nanocomposite. A Fe_2O_3-GO support showed higher surface area and thermal stability. Both the Au/Fe_2O_3-GO and the Au/Fe_3O_4 nanocomposites exhibited higher catalytic activity and reusability for the reduction of 4-nitrophenol. The present findings may open up a new aspect in the development of high-performance metal/Fe_2O_3-GO nanocomposites, which will be useful in heterogeneous catalysis.

Acknowledgements

This research was supported by Basic Science Research Program through the National Research Foundation of Korea (NRF) funded by the Ministry of Science, ICT & Future Planning (No.2013R1A1A1A05006634). K. H. P thanks to the TJ Park Junior Faculty Fellowship and LG Yonam Foundation. H. W thanks to the Dr. Yunhyeong Jang (Nextron, Republic of Korea) for AFM measurements.

Notes and references

[a] Department of Chemistry and Chemistry Institute for Functional Materials, Pusan National University, Busan 609-735, Korea. E-mail: chemistry@pusan.ac.kr; Tel.:+82-51-510-2238; Fax: +82-51-980-5200.

[b] Department of Physics, Pusan National University, Busan 609-735, Korea.

† Electronic Supplementary Information (ESI) available: [Detailed experimental procedures; DFM, XPS, surface areas, pore volumes and pore diameters]. See DOI: 10.1039/c000000x/

1. T. Mori, T. Watanuki and T. Kashiwaguru, *Environ. Toxicol.*, 2007, **22,** 58.
2. Y.-C. Tsao, S. Rej, C.-Y. Chiu and M. H. Huang, *J. Am. Chem. Soc.*, 2014, **136,** 396.
3. J. Wei, H. Wang, Y. Deng, Z. Sun, L. Shi, B. Tu, M. Luqman and D. Zhao, *J. Am. Chem. Soc.*, 2011, **133,** 20369.
4. K. Bramhaiah and N. S. John, *RSC Adv.,* 2013, **3,** 7765.
5. N. Zhang, X. Yu, J. Hu, F. Xuea and E. Ding, *RSC Adv.,* 2013, **3,** 13740.
6. Y. Tang, Z. Jiang, Q. Tay, J. Deng, Y. Lai, D. Gong, Z. Dong and Z. Chen, *RSC Adv.,* 2012, **2,** 9406.
7. A. M. Karim, V. Prasad, G. Mpourmpakis, W. W. Lonergan, A. I. Frenkel, J. G. Chen and D. G. Vlachos, *J. Am. Chem. Soc.*, 2009, **131,** 12230.
8. Y. Deng, Y. Cai, Z. Sun, J. Liu, C. Liu, J. Wei, W. Li, C. Liu, Y. Wang and D. Zhao, *J. Am. Chem. Soc.*, 2010, **132,** 8466.
9. G. M. Scheuermann, L. Rumi, P. Steurer, W. Bannwarth and R. Mülhaupt, *J. Am. Chem. Soc.,* 2009, **131,** 8262.
10. M. Lamblin, L. N. Hardy, J. C. Hierso, E. Fouquet and F. X. Felpin, *Adv. Synth. Catal.,* 2010, **352,** 33.
11. S. W. Kim, M. Kim, W. Y. Lee and T. Hyeon, *J. Am. Chem. Soc.*, 2002, **124,** 7642.
12. S. Y. Gan and M. Chow, *J. Mater. Chem.,* 2004, **14,** 2781.
13. P. V. Kamat, *J. Phys. Chem. Lett.,* 2011, **2,** 242.
14. D. Su, H.-J. Ahn and G. Wang, *Chem. Commun.,* 2013, **49,** 3131.
15. H. Xu, Q. Yang, F. Li, L. Tang, S. Gao, B. Jiang, X. Zhao, L. Wang and C. Fan, *Analyst,* 2013, **138,** 2678.
16. B. Liu, W. Zhang, F. Yang, H. Feng and X. Yang, *J. Phys. Chem. C*, 2011, **115,** 15875.
17. J. I. Paredes, S. Villar-Rodil, A. Martınez-Alonso and J. M. D. Tascon, *Langmuir,* 2008, **24,** 10560.
18. V. Petkova, Y. Pelovski, D. Paneva and I. Mitov, *J. Therm. Anal. Calorim.,* 2011, **105,** 793.
19. A. P. Grosvenor, B. A. Kobe, M. C. Biesinger, N. S. McIntyre, *Surf. Interface Anal.,* 2004, **36,** 1564.
20. D. Yang, A. Velamakanni, G. Bozoklu, S. Park, M. Stoller, R. D. Piner, S. Stankovich, I. Jung, D. A. Field, C. A. Ventrice Jr. and R. S. Ruoff, *Carbon,* 2009, **47,** 145.
21. R. Massart, *IEEE Trans, Magn.,* 1981, **17,** 1247.
22. J.-B. Moussy, *J. Phys. D: Appl. Phys.,* 2013, **46,** 143001.
23. M. Turner, V. B. Golovko, O. P. H. Vaughan, P. Abdulkin, A. Berenguer-Murcia, M. S. Tikhov, B. F. G. Johnson and R. M. Lambert, *Nature,* 2008, **454,** 981.
24. X. Meng, B. Li, X. Ren, L. Tan, Z. Huang and F. Tang, *J. Mater. Chem. A,* 2013, **1,** 10513.
25. X. Chen, Z. Cai, X. Chen and M. Oyama, *J. Mater. Chem. A,* 2014, **2,** 5668.
26. C. Wang, H. Daimon and S. Sun, *Nano Lett.,* 2009, **9,** 1493.
27. Z. Liu, X. Gong, J. Kohanoff, C. Sanchez and P. Hu, *Phys. Rev. Lett.*, 2003, **91,** 266102.
28. C. W. Corti, R. J. Holliday and D. T. Thompson, *Appl. Catal. A,* 2005, **291,** 253.